Magnetic fabrics and compositional evidence for the construction of the Caleu pluton by multiple injections, Coastal Range of central Chile

Miguel A. Parada[a,*], Pierrick Roperch[a,b], Claudio Guiresse[a], Ernesto Ramírez[a]

[a]*Departamento de Geología, Universidad de Chile, Casilla 13518, Correo 21, Santiago, Chile*
[b]*Institut de Recherche pour le Development (IRD), Casilla 5390, Correo Central, Santiago, Chile*

Abstract

The Caleu pluton, which is located in the Coastal Range of central Chile, consists of three N–S elongated lithologic zones which define an across-pluton compositional variation characterized by a westward increase in SiO_2 content, the Gabbro-Diorite (GDZ), Tonalite (TZ) and Granodiorite (GZ) Zones. A total of 547 cores were drilled at 68 sites within the different zones to carry out magnetic fabric and paleomagnetic studies. The highest values of magnetic susceptibility and remanent magnetization are found in the GDZ (0.04–0.1 SI), whereas the lowest values are observed in the GZ (0.01–0.02 SI). This is consistent with the significant decrease in magnetite content from the GDZ to the GZ. The dips of the magnetic foliation planes are steep within GDZ and TZ, and shallower dips are observed in GZ. Magnetic foliations along some borders of the pluton are parallel to the corresponding contacts. The parallelism observed between the magnetic foliations and the contacts between zones suggests that these zones have recorded the same mechanism of emplacement at the magmatic state. The peculiar foliation pattern observed in the central parts of TZ and GZ is attributed to a lobe-like structure that was acquired during the late stages of emplacement and inflation.

The distinct compositional characteristics of these three zones were not acquired in situ. Rather they were emplaced successively from mafic to felsic from a subjacent stratified sill-like magma reservoir, which was filled after tilting of the host volcanic succession. The rapid upward transport of these melts of different compositions up to a shallow depth is attested by both the equilibration pressure of late magmatic hornblende (~200 MPa) and the pressure of early magmatic epidote crystallization (~500–600 MPa). We conclude that space was created by lateral flow propagation, in which the intrusion of later pulses pushed earlier ones away from the feeder system, followed by roof lifting and possibly floor depression.

Keywords: Granitoids; Coastal range; Chile; Magnetic fabric; Paleomagnetism; Emplacement

* Corresponding author.
E-mail address: maparada@cec.uchile.cl (M.A. Parada).

1. Introduction

The discussion on the mechanism of granite magma emplacement has been shifted from the classical stoping, block foundering and expansion of a single episode to that models that recognize a key role played by tectonism to provide the space in the crust for incoming magma pulses (cf. Hutton, 1988). Moreover, field studies on mid- and upper-crustal granite plutons of different tectonic settings combined with modelling of emplacement mechanisms have favoured the model in which a laccolith is fed by vertical dikes, and developed mainly through a mechanism of space generation dominated by roof uplift and/or floor depression (e.g. Bridgewater et al., 1974; Nédelec et al., 1994; Cruden and Launeau, 1994; Petford, 1996; McCaffrey and Petford, 1997; Benn et al., 1998; Grocott et al., 1999; Brown and McClelland, 2000; Petford et al., 2000; McNulty et al., 2000). There are few case studies on pluton emplacement mechanism in the Andes. Cauldron subsidence and fluidization have been invoked as a mechanism of subhorizontal intrusion in the Coastal Batholith of Peru (Myers, 1975). Grocott et al. (1994) conclude that the Mesozoic pluton emplacements at 26–27°S, northern Chile, took place during an extensional regime and would have been localized at ramps within dilatational jogs. In the southern Chilean Andes, Skarmeta and Castelli (1997) provide evidence of roof uplift associated with the emplacement of the Torres del Paine laccolith. The present study considers the processes involved in the construction of the Caleu pluton, a typical Andean post-tectonic and shallow-emplaced pluton, based on the combination of magnetic fabrics and geochemical/petrological results. We selected this pluton because of its good exposures in more than 1400 of vertical relief, and its particular asymmetric rock distribution in elongated zones of lateral increasing SiO_2 content (Fig. 1).

The anisotropy of magnetic susceptibility (AMS) is a powerful tool to investigate the internal structures, or fabric of plutons where the macroscopic preferred mineral orientation is poorly expressed or absent (Bouchez, 1997). Hence, the mechanism of magma emplacement, or magma flow in a growing pluton can be derived with good confidence (Bouchez, 2000). Such a study has been undertaken in the Caleu pluton based on AMS measurements at 63 sites, along with structural observations in order to distinguish magmatic flow from high temperature subsolidus flow in the pluton. The geochemical investigation presented here aims at relating the compositional variations of the pluton with its mechanism of emplacement. We provide evidence indicating that the dominant processes in the construction of the pluton were: (1) upward magma transport by dikes from a subjacent reservoir, (2) episodic lateral magma intrusions of distinct compositions at the site of emplacement, and (3) thickening of the pluton by inflation to accommodate the increasing volume of magma.

2. The Caleu pluton

2.1. Geological setting

The Caleu pluton, located in the Coastal Range of central Chile ca. 40 km northwest of Santiago, corresponds to the latest event of the Early Cretaceous magmatism, which gave rise to one of the largest Andean magmatic provinces extending as a continuous belt from 27°S to 34°S. The Early Cretaceous magmatism derived from one of the most isotopically (Sr–Nd) depleted sources identified in the Chilean Andes (cf. Parada et al., 1999) and is associated with a regional extensional regime (Vergara et al., 1995) that yielded a crustal thinning.

The depth of the Caleu pluton emplacement has been estimated to be equivalent to a pressure of ~200 MPa by using the Al-in-hornblende geobarometer in more than 10 representative samples containing quartz, plagioclase, K-feldspar, hornblende, biotite, titanite and magnetite (Parada et al., 2002). Its volcano-sedimentary envelope, deposited in an Early Cretaceous subsiding basin (Vergara et al., 1995), is found to be tilted at about 25–50° to the east. It is made of the following formations, from older to younger: Horqueta, Lo Prado, Veta Negra and Las Chilcas. Horqueta Formation includes intermediate and acid lavas and continental sandstones; Lo Prado Formation is mainly formed by rhyolites, felsic tuffs and limestones; Veta Negra Formation corresponds to

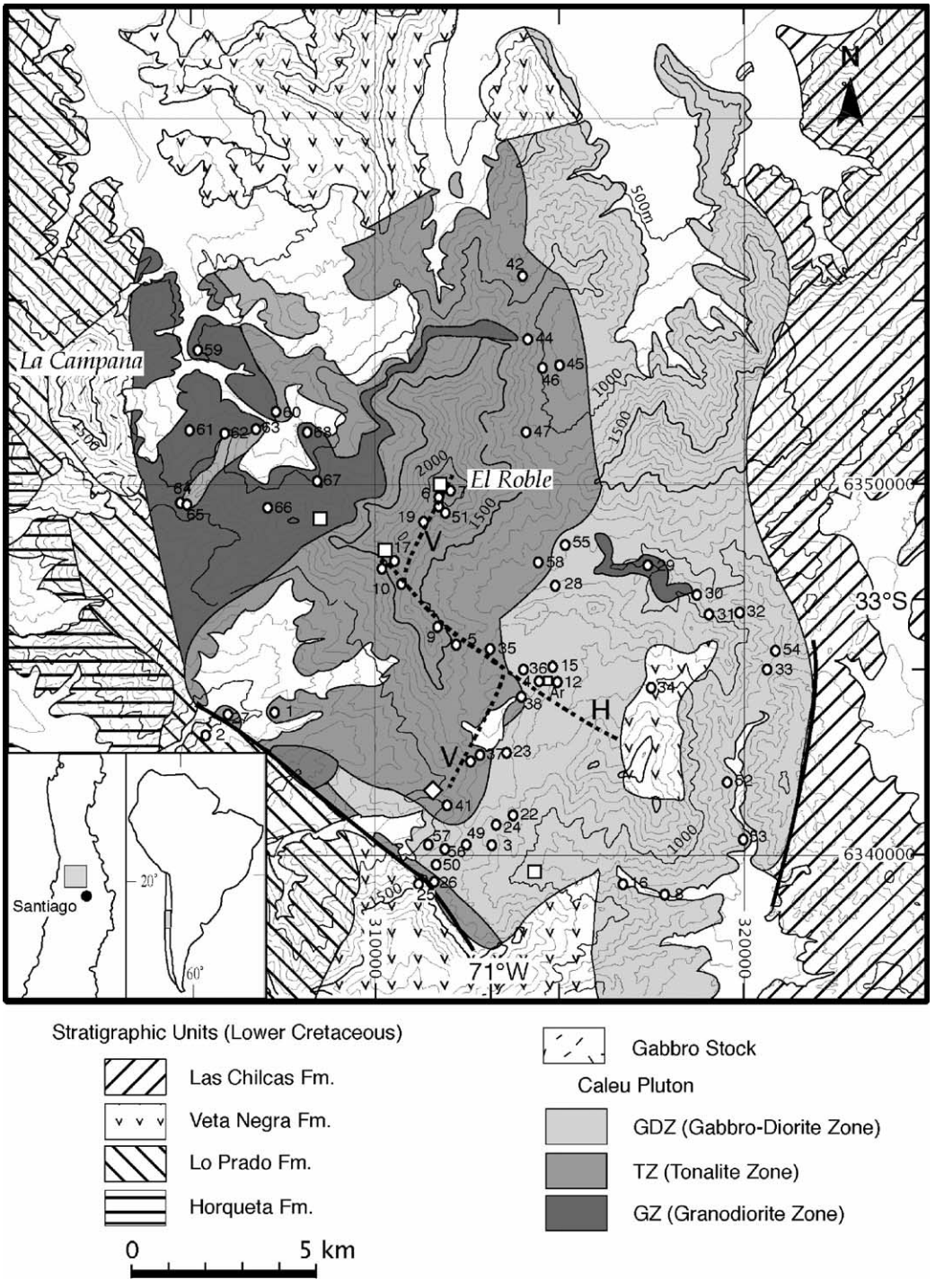

Fig. 1. Simplified geological map of the Caleu pluton region. Circles indicate the location of the paleomagnetic sites. Locations of subhorizontal (H) and vertical (V) geochemical traverses are shown. Open circles=paleomagnetic sites; open squares=Ar–Ar geochronologic sites; open diamonds=U–Pb geochronologic sites.

a ca. 10-km-thick pile of basalts and basaltic andesites; Las Chilcas Formation is a succession of limestone, red sandstones and volcano-sedimentary breccias and conglomerates. The western margin of the pluton is the contact with the La Campana gabbro stock and with felsic volcanic rocks and limestone of the Lo Prado Formation. The southwestern and southern margins of the pluton are defined by a NW–SE fault and by the intrusive contact with basaltic rocks of the Veta Negra Formation, respectively. The eastern margin is defined either by a N–S fault or by sills of granitoids injected into the volcano-sedimentary strata of the Las Chilcas Formation. Testimonies of the roof have been observed close to the southern end of the pluton (Fig 1), consisting of a pile of basaltic andesite of the Veta Negra Formation, and whose lower strata are interfingered with granitoid sheets.

A U–Pb date of 94.5±2.2 Ma from a gabbro-diorite facies is similar to the Ar–Ar cooling ages obtained on hornblende (93.2±1.1 to 95.0±2.8 Ma), biotite (93.4±0.8 to 96.0±0.8 Ma) and plagioclase (94.0±0.3 Ma) of more felsic facies of the pluton, suggesting a very rapid subsolidus cooling (Parada et al., 2001).

2.2. Lithologic zones

The pluton is subrectangular in plant view and covers an area of about 340 km^2. It consists of three N–S elongated lithologic zones (Fig. 1) with westward-increasing SiO_2 contents: a Gabbro-Diorite Zone (GDZ), a Tonalite Zone (TZ) and a Granodiorite Zone (GZ).

The GDZ occupies 140 km^2 of the eastern part of the pluton and includes coarse-grained gabbros, diorites and quartz-monzodiorites, which locally exhibit ortho- and meso-cumulate oriented plagioclase, sub-ophitic pyroxene and interstitial K-feldspar. Apatite, magnetite and ilmenite are the more common accessory phases. Subidiomorphic and slightly resorbed crystals (0.1–0.3 mm in size) of magmatic epidote armoured by amphibole, biotite or quartz were also found as an accessory phase. Compositional variations towards more felsic (quartz-monzonite) and metric scale fine-grained marginal facies are recognized along the southern contact of the pluton, between the GDZ and the Lo Prado, Veta Negra and

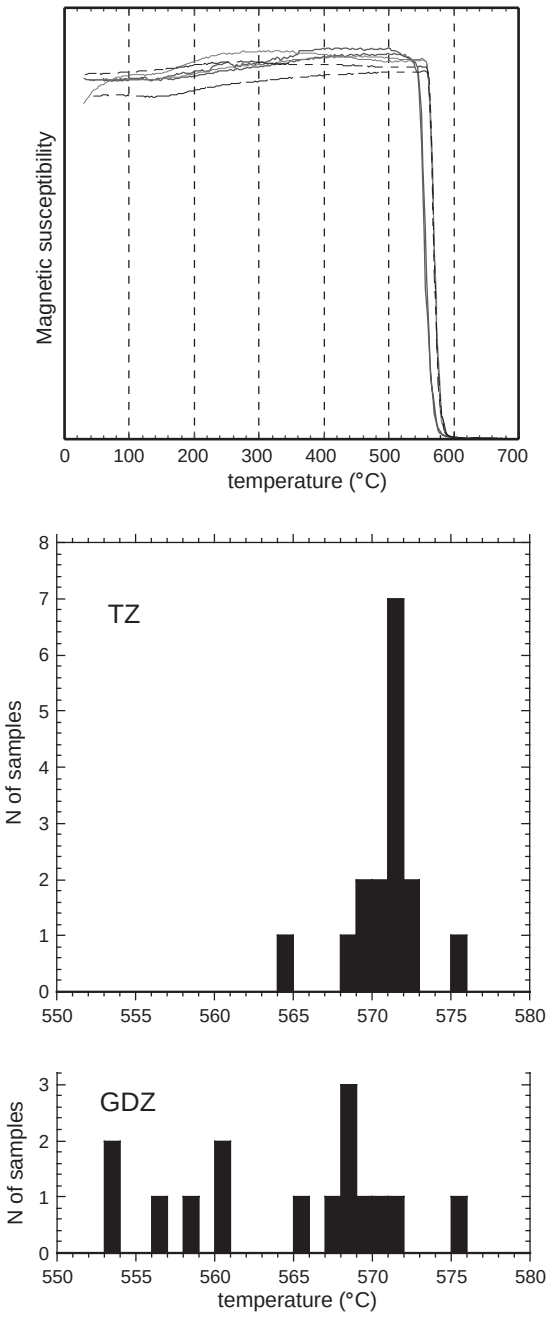

Fig. 2. Top: Examples of thermomagnetic experiments in low field showing well-defined Curie temperatures and almost reversible heating and cooling curves. Bottom: Histogram of Curie temperatures for TZ and GZ units. Most samples have Curie temperatures showing pure magnetite except in GDZ where Ti-poor titanomagnetites are indicated by Curie temperatures in between 550 and 565 °C.

Table 1
Site locations and paleomagnetic results

Unit	Site	UTM east	UTM north	*J*	K		*N*	Dec	Inc	α95	*k*
GDZ	3	313249	6340232	1.58	0.072	L	7	10.8	−50.1	4.0	227
GDZ	4	314452	6344700	2.65	0.065	L	6	8.6	−51.8	3.3	407
GDZ	8	317883	6338893	0.82	0.117	L	8	17.4	−54.4	3.5	246
GDZ	11	314740	6345119	2.62	0.043	L	11	10.1	−51.5	2.7	290
GDZ	12	314945	6344691	2.52	0.041	20	7	13.3	−49.5	4.1	220
GDZ	13	314825	6345251	1.62	0.042	20	9	10.9	−50.6	1.7	963
GDZ	14	314822	6344978	0.87	0.085	20	4	8.0	−49.9	6.9	179
GDZ	15	314861	6345063	1.18	0.056	20	7	3.2	−50.6	3.9	243
GDZ	16	316780	6339170	1.62	0.123	L	4	7.7	−57.0	11.3	67
GDZ	22	313750	6341059	2.75	0.045	L	8	35.1	−52.2	2.5	482
GDZ	23	313590	6342755	6.59	0.074	L	8	14.4	−52.5	7.1	62
GDZ	24	313296	6340778	0.74	0.065	L	10	9.0	−53.7	6.1	63
GDZ	28	314932	6347267	1.05	0.051	L	8	12.8	−59.9	4.2	171
GDZ	30	318745	6347021	1.28	0.061	L	6	16.7	−60.2	4.0	279
GDZ	31	319105	6346495	0.68	0.044	L	7	356.2	−64.3	4.9	151
GDZ	32	319899	6346545	0.35	0.035	L	7	352.0	−56.2	3.6	279
GDZ	33	320629	6344994	0.32	0.040	L	5	328.3	−56.5	7.7	100
GDZ	36	314028	6344996	0.36	0.053	L	7	1.1	−54.1	5.4	127
GDZ	38	314008	6344277	1.88	0.045	L	10	14.6	−55.3	2.9	287
GDZ	49	312474	6340268	0.21	0.063	L	5	354.2	−39.7	4.6	283
GDZ	50	311687	6339700	0.30	0.021	L	10	4.0	−50.6	3.2	227
GDZ	52	319587	6341973	1.38	0.057	20	8	340.8	−58.4	4.0	192
GDZ	53	319975	6340418	0.28	0.028			–	–	–	–
GDZ	54	320906	6345505	0.42	0.042	20	6	288.1	−45.7	9.4	52
GDZ	55	315161	6348380	1.34	0.05	20	5	16.9	−59.0	5.8	173
GDZ	56	311880	6340135	0.28	0.035	20	6	0.0	−57.2	7.5	81
GDZ	57	311465	6340283	0.87	0.053	20	5	10.7	−50.6	8.7	78
Average GDZ over 22 sites							22	9.7	−53.7	2.8	127
TZ	1	307312	6343825	0.06	0.017	L	7	18.8	−56.0	14.1	19
TZ	5	312228	6345697	0.30	0.027	L	6	31.6	−64.7	3.4	378
TZ	6	311758	6349659	3.19	0.030	L	6	20.9	−59.7	3.3	412
TZ	7	312076	6349826	1.12	0.030	L	6	20.0	−55.0	4.9	186
TZ	9	311720	6346184	0.25	0.029	L	7	28.3	−52.0	5.1	138
TZ	10	310750	6347351	0.13	0.026	L	16	11.2	−60.4	2.9	162
TZ	17	310560	6347920	0.21	0.032	L	8	11.9	−59.5	2.6	462
TZ	18	310219	6347716	0.44	0.005			Not	In situ		
TZ	19	311364	6349010	0.14	0.036	L	4	29.2	−55.3	10.0	84
TZ	20	311760	6349400	0.48	0.031						
TZ	26	311568	6339213	0.25	0.031	L	4	4.1	−49.1	7.3	160
TZ	27	305928	6343685	0.53	0.027	L	6	9.5	−54.6	4.8	198
TZ	35	313157	6345585	0.45	0.028	L	6	25.9	−58.6	6.2	116
TZ	37	312855	6342703	0.34	0.025	L	7	9.0	−51.8	4.2	204
TZ	39	315419	6349955	0.41	0.025			Not	In situ		
TZ	40	312619	6342519	0.28	0.028			Not	In situ		
TZ	41	311984	6341285	0.27	0.019	L	7	18.8	−60.7	6.6	83
TZ	42	314045	6355655	0.16	0.025	L	10	15.7	−54.6	5.3	85
TZ	43	314384	6355100	0.09	0.023						
TZ	44	314175	6353965	0.16	0.032	L	8	3.5	−54.9	3.2	298
TZ	45	315012	6353271	0.12	0.029	L	8	6.8	−57.9	6.7	70
TZ	46	314540	6353202	0.08	0.022	L	6	11.0	−52.3	4.9	184
TZ	47	314128	6351437	0.72	0.021	L	8	18.1	−57.7	3.6	238

(continued on next page)

Table 1 (*continued*)

Unit	Site	UTM east	UTM north	*J*	K		*N*	Dec	Inc	α95	*k*
TZ	51	311935	6349233	0.40	0.030	20	9	18	−55.6	3.8	186
TZ	58	314470	6347880	0.38	0.034						
Average TZ over 19 sites							19	16.1	−56.6	2.5	185
GZ	29	317443	6347782	0.56	0.0006	L	6	15.3	−64.4	3.4	392
GZ	59	305215	6353645	0.06	0.004	20		–	–	–	–
GZ	60	307323	6351964	0.05	0.014	20	8	0.8	−62.6	6.6	71
GZ	61	304982	6351505	0.06	0.011	20	5	358.2	−55.0	8.7	78
GZ	62	305918	6351380	0.16	0.012	20	11	11.5	−58.7	5.3	76
GZ	63	306771	6351535	0.14	0.017	20	8	12.5	−50.6	5.6	99
GZ	64	304735	6349555	0.08	0.025	20		–	–	–	–
GZ	65	304883	6349478	0.14	0.023	20	7	13.6	−54.5	6.2	95
GZ	66	307090	6349374	0.16	0.012	20	8	17.4	−58.7	6.5	73
GZ	67	308411	6350124	0.03	0.016	20		–	–	–	–
GZ	68	308190	6351432	0.008	0.001	20		–	–	–	–
Average GZ over 7 sites							7	9.9	−58.0	4.6	171
Average GDZ, TZ and GZ over 48 sites							48	12.2	−55.5	1.8	138
VN	34	317515	6344505	4.20	0.097	L	4	7.9	−54.0	2.3	154
VN	25	311291	6339237	0.57	0.108	L	9	18.9	−53.5	4.9	109
LP	02	307312	6343825	0.16	0.009	L	6	19.5	−58.9	5.4	156
Average GDZ, TZ, GZ, LP and VN over 51 sites							51	12.4	−55.5	1.7	143

J: NRM intensity in A/m; *K*: magnetic susceptibility in SI units; *N*: number of samples used in the calculation of the mean direction. L means that the characteristic direction for each sample was determined by a least-square fit through the origin. In the other cases, the site-mean direction was determined by Fisher statistics at 20 mT AF demagnetization step. Dec, Inc: Mean declination and inclination in situ. α95: Semi-angle of 95% of confidence. *k*: Fisher's precision parameter.

Las Chilcas formations. Similar lithological variations are recognized towards the eastern margin of the pluton, but in these cases sheets of felsic granitoids are interbedded with the host volcano-sedimentary strata of the Las Chilcas Formation.

Tonalites and quartz-diorites occupy the central part of the pluton (TZ) forming a N–S elongated body of about 70 km^2. In most places, towards the contact with GDZ, the TZ rocks exhibit a decrease in both the color index and grain size from coarse- to medium-grained. However, small batches of TZ quartz-diorite intruding GDZ rocks have been observed locally. Macroscopic mafic mineral preferred orientations are seldom observed. Amphiboles, biotites and Fe–Ti oxides occur as crystal aggregates and apatite, magnetite, titanite and zircon are common accessory phases. Likewise the GDZ, some rocks of the TZ also have small subhidiomorphic crystals of early magmatic epidote enclosed in biotite, hornblende and quartz. Resorption of about 0.2 mm is observed in rims of some of this magmatic epidote. A distinct feature of this TZ is the presence of rounded microdiorite/microgabbro enclaves ranging from 5 to 40 cm, whose spatial distribution is variable, being more abundant in the central part of TZ than in its periphery.

Hornblende–biotite granodiorites (GZ) cover 30 km^2 of the western part of the body. The granodiorites are leucocratic, have no macroscopic mineral fabric, and present fine- to medium-grained porphyric textures. Common accessory minerals are magnetite, titanite, zircon and allanite. A ~100-m-thick granodioritic dike, hosted within TZ, is recognized as an extension of GZ towards the east. A brecciated intrusive contact between GZ and TZ is locally observed, consisting in subangular to rounded fragments of tonalite within a granodioritic matrix. Intrusions of isolated metric-scale GZ bodies

into GDZ also occur in the eastern part of the pluton.

2.3. Structural features

The pluton as a whole is macroscopically isotropic. However, a strong plastic deformation marked by a N40°W/65°–80°SW foliation and a N40°–50°E-trending stretching lineation is locally observed in a zone a few meters wide along the southwestern margin of the pluton. This highly deformed zone belongs to the NW–SE-trending fault contact (Fig. 1) separating the pluton from the Lo Prado and Veta Negra formations. In the westernmost exposures of GZ a tectonic–magmatic N–S-striking foliation parallel to the western margin can be locally evidenced in the field. Some mafic varieties of the central GDZ exhibit in the field a subhorizontal NE–SW trending mineral lineation, defined by the alignment of euhedral prismatic plagioclase and amphibole crystals. In these rocks the absence of submagmatic microfactures (cf. Bouchez et al., 1992), solid-state deformation textural features and extensional microfractures due to mineral stretching allow us to interpret this mineral fabric as purely magmatic in origin.

3. Paleomagnetic sampling and methods

547 cores were drilled at 68 different sites within the pluton (Fig. 1). In most cases, samples were oriented with both magnetic and sun compasses. The natural remanent magnetization (NRM) was measured with Molspin or JR5 Agico spinner magnetometers, and the magnetic susceptibility was measured with a Bartington susceptibility meter. Alternating field (AF) demagnetization was performed with a Molspin AF demagnetizer. The anisotropy of magnetic susceptibility (AMS) was measured with the KLY3S kappabridge (Agico). Few samples from two sites of the GDZ yielding magnetic susceptibilities higher than 0.1 SI could not be measured.

Variation of the magnetic susceptibility versus temperature (Fig. 2) was performed with the KLY3 susceptibility meter and CS3 furnace from Agico. Isothermal remanent magnetizations (IRM) were imparted with the ASC impulse magnetizer allowing us to determine saturation remanent magnetizations (Jrs) and remanent coercitive fields (Hcr).

4. Magnetic mineralogy

4.1. Paramagnetic mineralogy

Amphibole phenocrysts of GDZ and TZ are Mg-hornblende formed lately with respect to clinopyroxene and early plagioclase, but crystallized along with quartz, biotite and late plagioclase. Amphiboles from GZ occur as phenocrysts and form part of the groundmass. They correspond to Mg- and Fe-hornblende, although Fe-edenites were also found (Parada et al., 2002). The average modes of amphiboles in GDZ, TZ and GZ are 12.3, 10.6 and 2.7 vol.%, respectively.

Biotites from the three granitoid zones occur as euhedral to subhedral ~0.1–1.0 mm crystals or as crystal clots of similar size often associated with hornblende and magnetite. Biotite phenocrysts as large as 3 mm locally occur in GDZ and TZ. The mode of biotite in TZ (10.6 vol.%) is about three times that observed in GDZ and GZ. The mean modal ratios between hornblende and biotite are 4.2, 1.1 and 0.8 for GDZ, TZ and GZ, respectively. Mean Fe/(FeO+MgO) compositions of biotite from

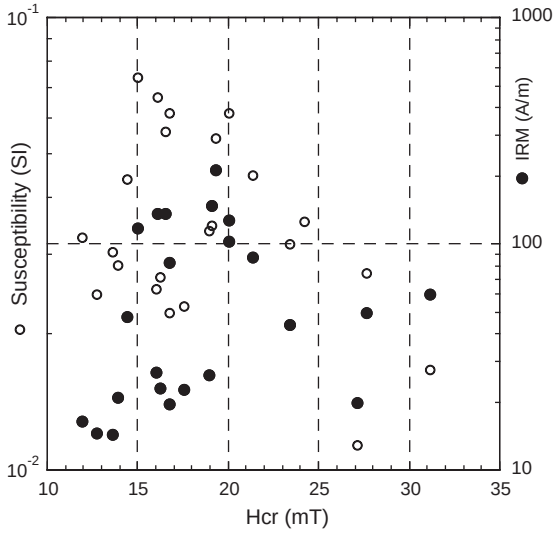

Fig. 3. Comparison of magnetic susceptibility and saturation IRM versus Hcr for 23 samples from the three units.

GDZ, TZ and GZ are 0.39, 0.44 and 0.49, respectively.

4.2. Ferromagnetic mineralogy

Magnetite is the most abundant Fe–Ti oxide, hence, the main contributor to the magnetic susceptibility. High magnetic susceptibilities (Table 1), isothermal remanent magnetization and thermomagnetic experiments (Fig. 2) indicate that magnetite is the main remanent magnetic carrier within the pluton.

The modal contents of magnetite and ilmenite grains progressively decrease from an average of 2.3% in GDZ to 1.4% in TZ to 0.6% in GZ. Electron microprobe analyses of these grains (Larrondo, 2002) show that most of them correspond to nearly pure magnetite. Unlike magnetite from TZ and GZ, magnetite from GDZ has substantially lower MnO content. Ilmenite grains are very scarce in the whole pluton and the few crystals analyzed gave X_{il} of about 0.97. Thermomagnetic measurements in low field provided Curie temperatures (inflection point) about 570 °C, which indicate nearly pure magnetite in agreement with microprobe analyses. Only a few samples from GDZ have Curie temperatures around 550 °C (Fig. 2).

Optical microscope observations indicate that the size of the Fe–Ti oxides varies between 0.05 and 1.0 mm. They appear either as euhedral or subhedral

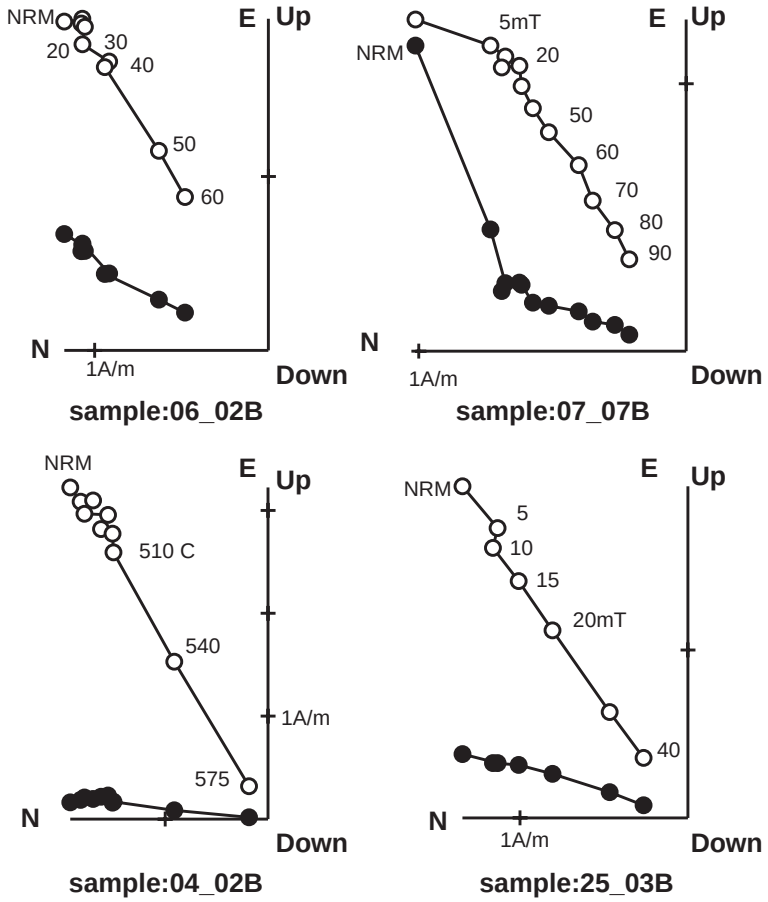

Fig. 4. Orthogonal projections (in situ) of alternating field and thermal demagnetization data showing well-defined characteristic vectors. Solid (open) circles correspond to projection into the horizontal (vertical) plane.

individual crystals commonly included in plagioclase crystals or as aggregates of anhedral crystals spatially associated with mafic silicates. However, more than 50% of the samples have medium destructive field (MDF) values of natural remanent magnetization (NRM) larger than 20 mT. Hcr values are usually higher than 15 mT and are not correlated with magnetic susceptibility or saturation IRM (Fig. 3). These observations suggest that a significant part of the NRM is carried by small pseudo-single domain grains possibly included in plagioclase crystals.

Intensity of remanent magnetizations and magnetic susceptibilities correlate with the compositional zoning observed in the pluton (Table 1), the highest susceptibility values being found in GDZ (0.04–0.1 SI) and the lowest in GZ (0.01–0.02 SI). This is consistent with the significant decrease in magnetite content from GDZ to GZ.

5. Remanent magnetizations—characteristic directions

One or two specimens per site were progressively AF demagnetized (Fig. 4) and 22 samples were progressively thermally demagnetized. Because the pilot study demonstrated that the secondary magnetizations were, in most cases, destroyed by AF demagnetization at about 10 mT, the other specimens were AF demagnetized at steps 10, 20 and 30 mT. Remanent magnetization of samples

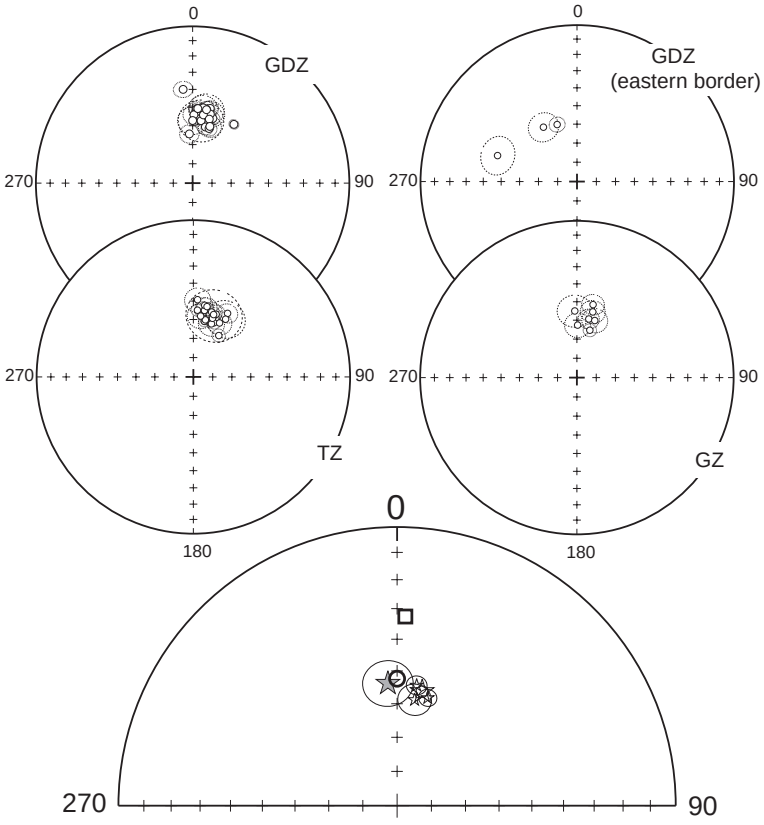

Fig. 5. Top: Equal-area projection of site-mean characteristic paleomagnetic directions (open circles) with 95% confidence angle. Bottom: Comparison of mean-site directions for GDZ, TZ and GZ (small stars) with expected mid-Cretaceous direction from the Besse and Courtillot APWP (2002) (grey star). Large open star is the mean direction determined for the whole pluton. Square is present-day field and large circle is the geocentric axial dipole direction. Open symbols are projections in the upper hemisphere.

from GDZ is more stable than the remanent magnetization of samples from GZ. At all sites but one from GDZ, characteristic magnetizations were determined, whereas 4 sites out of 11 from GZ were rejected because of a large dispersion upon AF demagnetization.

Normal polarity of the remanent magnetization is observed at all sites. A well-defined characteristic magnetization was determined at 52 sites within the pluton and at 3 sites in andesites of the host rocks (one site at Lo Prado Formation and two sites at Veta Negra Formation) (Table 1; Fig. 5). Because the present-day field in central Chile is characterized by low inclination (Fig. 5), we can easily discard the hypothesis that the observed magnetizations record the present-day field. On the other hand, the direction of an overprint in the Brunhes field is not different from the expected one during the Late Cretaceous. However, high unblocking temperatures observed on pilot samples and high MDF values demonstrate that these characteristic magnetizations were acquired upon cooling of the pluton in agreement with a pluton emplacement during the Cretaceous long normal superchron. Unlike many paleomagnetic studies in plutons like the Mount Givens study (Gilder and McNulty, 1999), mean-site characteristic directions are well defined as shown by high values of the Fisher concentration parameter k (Table 1). The slight variations in the paleomagnetic declinations, observed among sites (Fig. 6), suggest

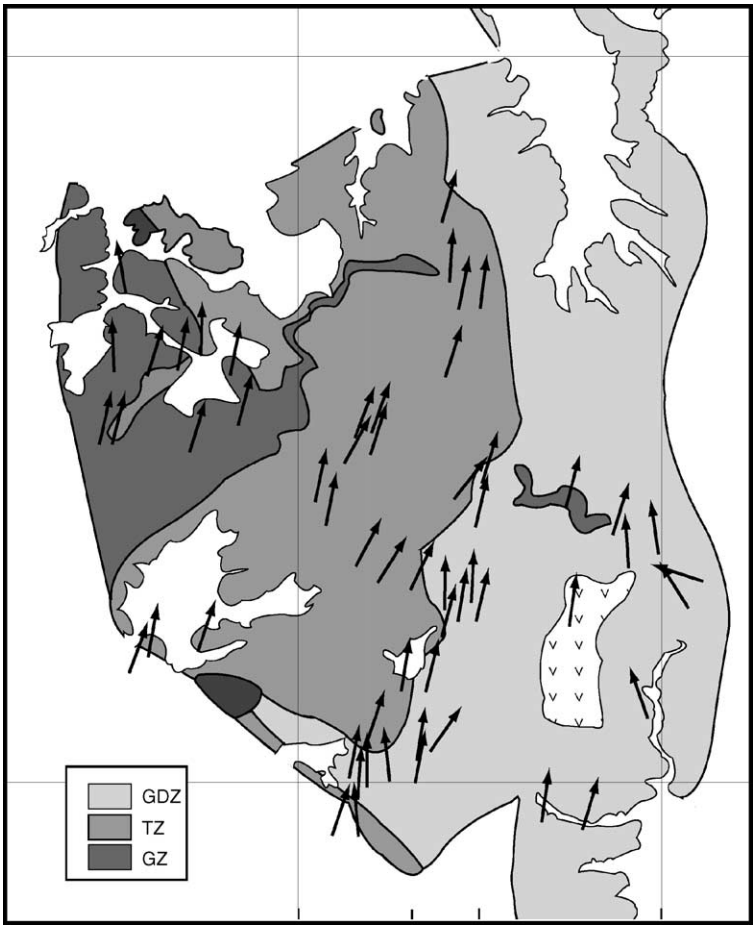

Fig. 6. Spatial variation of the paleomagnetic declinations within the pluton.

Table 2
AMS results

Site	N	K1	K2	K3	Direction of Kmax				Direction of Kmin				L (%)	F (%)	A (%)
					D	I	P1	P2	D	I	P1	P2			
GDZ unit															
3	12	1.048	0.977	0.975	266.8	75	6.6	2.6	125.9	11.7	72.2	6.1	7.2	0.3	7.5
4	9	1.047	1.029	0.924	47.4	71.7	26.5	5.3	297.9	6.3	6.9	5.5	1.7	11.4	13.3
8	3	1.037	0.992	0.971	312.4	51.3	71.4	39.8	186.8	25	87.6	42.9	4.6	2.2	6.9
11	10	1.044	1.041	0.915	255	75.9	62.2	3.5	114.6	10.9	12.3	3	0.4	13.7	14.1
12	7	1.027	1.016	0.958	333.2	31.1	63.3	13.5	132.3	57.1	18.7	10.5	1.1	6.1	7.2
13	10	1.042	1.020	0.938	333.6	73.7	20.7	10	114.1	12.7	12.2	11.7	2.1	8.8	11.1
14	6	1.082	1.006	0.913	256.8	54.6	11.2	7.9	44.8	31.1	13.3	5	7.5	10.2	18.5
15	7	1.059	1.024	0.918	232.9	70.5	11.7	3.4	117.6	8.6	13.2	3.9	3.4	11.5	15.3
16	6	1.024	1.017	0.959	249.2	20.1	42.3	3.7	353.8	34.6	4.8	3.5	0.7	6.1	6.8
22	9	1.030	1.001	0.970	249.2	53.8	14.4	6.4	46.6	34	23	4.8	2.9	3.2	6.2
23	10	1.026	1.014	0.960	331.3	58.6	27.8	8.5	96.6	19.4	13.3	8.8	1.1	5.7	6.8
24	10	1.047	0.994	0.959	231.8	66.5	10.1	6.5	100	16.2	19.5	8.3	5.3	3.7	9.2
28	8	1.036	0.994	0.970	3.1	65.6	7.3	3	161.2	22.9	20.2	4	4.1	2.5	6.8
30	6	1.014	1.008	0.978	212.5	44.5	63.8	17	109.7	12.7	22.3	13.3	0.5	3.1	3.7
31	8	1.006	1.003	0.991	170.1	11.8	62.1	19.1	74.2	26.3	19.8	18.8	0.3	1.3	1.6
32	7	1.007	1.004	0.989	189.3	78.2	68.2	24.3	284.7	1.1	28.2	19.3	0.3	1.4	1.8
33	7	1.016	0.995	0.989	193.7	57.4	19.1	11.1	306	13.6	38.2	9.2	2.1	0.6	2.8
36	8	1.025	1.017	0.958	20.4	37.5	51.1	8.5	110.5	0.1	16.4	8.4	0.8	6.1	7
38	11	1.024	1.007	0.969	200.4	18.9	23.9	6.4	292.7	6.7	35	6	1.8	3.9	5.7
49	9	1.013	0.998	0.989	181.1	49.7	44.9	20.2	322.5	33.5	48	21.1	1.5	0.9	2.4
50	10	1.040	1.000	0.960	187.6	73.2	7.8	4.8	76.5	6.2	16.6	4.6	4.1	4.2	8.4
52	9	1.006	1.001	0.993	152.5	16.9	50.3	19.8	284.2	65.5	33.1	24.8	0.4	0.8	1.3
53	6	1.007	1.002	0.991	138.5	0.8	58.5	11.7	47.7	44.7	39.5	20.3	0.5	1.1	1.5
54	7	1.008	0.998	0.993	48.6	20	40.3	12.1	297.4	44.8	33.8	8.5	1	0.5	1.5
55	5	1.025	0.993	0.982	200.4	77.2	23.7	14.1	90.2	4.5	68.1	20	3.1	1.1	4.3
56	7	1.048	0.997	0.954	112.2	81.8	27.3	8.3	223.6	3	20.8	14.2	5.1	4.5	9.8
57	7	1.077	1.008	0.915	218.8	70.8	7.8	5.2	55.7	18.4	12.2	4.4	6.8	10.2	17.7
TZ unit															
1	13	1.050	1.008	0.943	197.8	65.2	5.4	4.2	56.7	19.8	7.1	4	4.2	6.9	11.4
5	3	1.020	0.999	0.982	252.3	71.1	75.2	39.1	10.3	9.1	73.4	35.5	2.1	1.7	3.8
6	8	1.022	1.014	0.964	61.3	10.2	29.7	8.9	161.7	45.1	19.1	5.4	0.8	5.2	6
7	13	1.009	1.005	0.986	291.3	18.6	44.4	10.5	190.5	29.1	13.2	9.1	0.3	2	2.3
9	8	1.027	1.013	0.960	116.4	1.2	28.1	5.8	25.5	35.7	15.4	3.1	1.4	5.4	6.9
10	25	1.014	1.006	0.980	210.8	50.4	30.4	6.1	93.7	20.7	9.5	6.1	0.7	2.6	3.4
17	8	1.025	1.009	0.967	210.3	63.7	26.3	11.2	105.9	7	11.6	3.6	1.5	4.4	6
19	7	1.029	1.027	0.945	221.9	0.	78	10.5	131.9	31.6	20.4	7.5	0.2	8.7	8.9
20	4	1.018	1.004	0.978	246.3	5.1	60.3	15.9	144.6	66.4	65.7	18.7	1.5	2.6	4.1
26	6	1.034	1.011	0.955	189.7	58.3	41.2	14.5	47.2	26.2	18.2	11.5	2.3	5.9	8.3
27	7	1.046	1.005	0.949	230.4	68.1	8.6	5.6	43.1	21.7	10.4	5.5	4.1	5.8	10.1
35	6	1.027	1.024	0.949	192.2	33.6	78	6.6	291.6	13.9	11.5	5.3	0.3	7.9	8.2
37	7	1.020	1.015	0.966	237.4	54.1	50.1	2.6	139.6	5.6	8	1.9	0.5	5.1	5.6
41	7	1.010	1.004	0.986	90.6	4.2	46.6	15.2	180.7	2.1	17.5	11.1	0.6	1.9	2.5
42	12	1.011	0.997	0.992	336.3	4.3	27.1	17.8	244.8	20.1	66.1	21.6	1.5	0.4	1.9
43	8	1.012	0.998	0.990	165.2	48	45.2	17.6	9.3	39.5	67.4	33.3	1.3	0.8	2.2
44	11	1.023	0.996	0.981	24.4	29.7	8.2	5.9	236.3	56.1	10.8	7	2.7	1.5	4.2
45	9	1.040	0.993	0.966	92.5	62.1	12	10.1	261.6	27.5	10.9	6.7	4.7	2.8	7.7
46	9	1.018	1.003	0.978	7.5	11	13.3	9.2	271	30	17.6	9.7	1.5	2.6	4.1
47	8	1.015	1.010	0.975	75.1	40.7	60.6	8.4	283.5	45.6	21.5	6.2	0.4	3.6	4.1
51	11	1.018	1.011	0.971	252.6	65.9	41.7	11.2	31.1	18.5	11.3	7.2	0.7	4.1	4.8
58	7	1.024	1.013	0.963	273.8	69.4	52.5	9.7	14.2	3.9	29.1	9	1	5.2	6.3

(continued on next page)

Table 2 (*continued*)

Site	N	K1	K2	K3	Direction of Kmax				Direction of Kmin				*L* (%)	*F* (%)	*A* (%)
					D	I	P1	P2	D	I	P1	P2			
GZ unit															
29	6	1.008	1.002	0.991	271.9	74.5	38.5	10.8	119.2	13.8	28.1	10.9	0.6	1.1	1.7
59	5	1.025	1.016	0.960	291.3	37.9	76.3	7.5	132.2	50.2	17	8.1	0.9	5.8	6.8
60	9	1.025	1.000	0.974	16.1	14.8	9.5	3.4	173.8	74.1	19.2	6.2	2.5	2.6	5.2
61	5	1.016	1.008	0.976	247.4	29.8	53.2	11.6	127.6	41	24.3	6.8	0.8	3.3	4.1
62	15	1.022	1.003	0.975	22.2	2.7	20.5	7.9	117	60.8	30.6	6.8	1.9	2.9	4.9
63	11	1.026	0.996	0.977	1.1	44.5	27.9	13.5	155.6	42.5	41.9	19	3	2	5
64	8	1.029	1.006	0.965	282.5	49.7	39.8	16.3	55.1	29.9	24.9	11.1	2.3	4.2	6.6
65	6	1.024	1.010	0.966	260.3	32.5	26	19.7	77.5	57.5	25	6.2	1.4	4.6	6.1
66	8	1.016	0.999	0.985	327	31.1	28	12.5	132.4	58.1	56.3	9.8	1.6	1.5	3.1
67	8	1.044	1.040	0.916	18.4	0.3	60.3	9.2	108.7	36.8	11.2	6.6	0.4	13.5	13.9
68	8	1.022	0.998	0.980	54.7	9.8	22	11.1	200	78.2	36.5	9.6	2.5	1.8	4.3
LP and VN units															
34	2	nd	nd	nd	191.0	60.0	nd	nd	312.0	16.0	nd	nd	1.1	4.8	5.9
25	7	1.061	1.007	0.932	32.1	77	11.2	3.1	230.1	12.4	9.4	2.5	5.4	8	13.9
2	9	1.081	1.006	0.912	256.8	54.6	11.2	7.9	44.8	31.1	13.3	5.0	7.5	10.2	18.5

N: number of samples used in the site-mean normalized tensor calculation. K1, K2 and K3 are respectively the maximum, intermediate and minimum axes of the ellipsoid. D, I are the declination and inclination of Kmax and Kmin; P1 and P2 are the parameters of the ellipse of confidence around the mean directions. *L*, *F* and *A* correspond to the lineation, foliation and anisotropy parameters; *L*=[1−(kmax/kint)]*100; *F*=[1−(kint/kmin)]*100; *A*=[1−(kmax/kmin)]*100.

small deformations within the pluton. The most significant departures are observed in three sites near the eastern border of the pluton in agreement with field observations of local post-emplacement brittle deformation. Discarding these three sites, the average paleomagnetic direction for the remaining 48 sites within the pluton (declination: 12.2°; inclination: −55.5°; α95: 1.8°) is slightly different from the expected direction at 95 Ma determined from the new Apparent Polar Wander Path (Besse and Courtillot, 2002) (declination: 355.7°; inclination: −53.7°). The difference between the observed and the expected directions could result from a 10° to 20° tilting of the pluton toward the east. However, the remagnetized Lo Prado and Veta Negra dipping strata of the southwestern margin (dipping 40–50° at site 2 and nearly vertical at site 25) have the same in situ paleomagnetic direction as the one recorded in the adjacent plutonic rock, suggesting that the pluton probably intruded the host volcanic formations after their tilting. Taking into account the widespread clockwise rotations already evidenced several times along the Chilean forearc (Beck, 1998, Goguitchaichvili et al., 2000), our paleomagnetic results are best explained by a vertical-axis clockwise rotation of the Caleu pluton of 16.5°±6.7. A detailed paleomagnetic study of the Veta Negra volcanic Formation away from the pluton border is however needed to confirm this interpretation.

6. Magnetic fabrics

Five to ten samples were measured at each site (Table 2). Three examples of AMS tensors are shown in Fig. 7. No large spatial variations were observed at sites where the sampling was spread over a few tens of meters. This observation is consistent with the study of Olivier et al. (1997) showing that granite anisotropy is remarkably homogeneous at small scales. However, the shape of the ellipsoids may vary between samples from a single site even though the directions of the principal axis of the ellipsoids do not change (see examples of sites 3 and 35 in Fig. 7). Fifty percent of the samples have foliation parameters lower than 4% while 50% of the samples have lineations parameters lower than 2% (Fig. 8). Magnetic anisotropy does not correlate with magnetic susceptibility (Fig. 8) but shows significant spatial variations within the pluton. Low

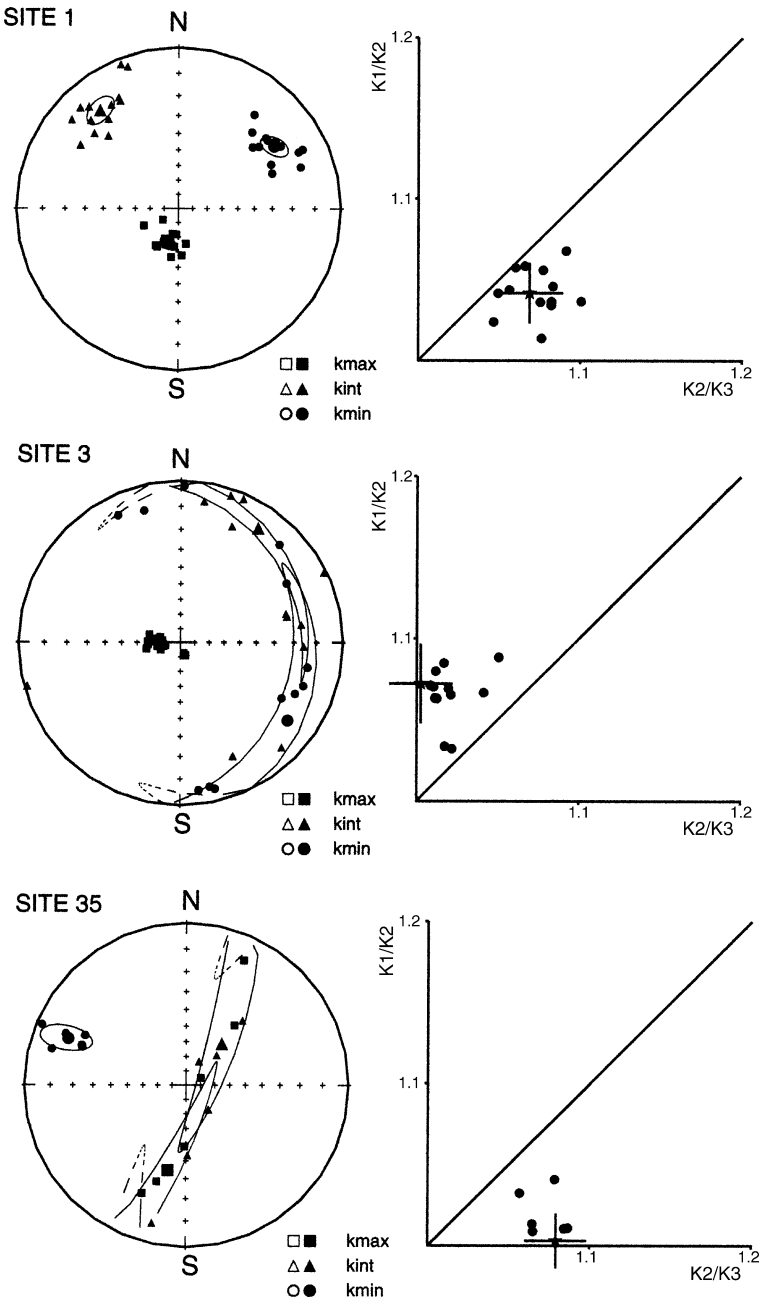

Fig. 7. Examples of AMS tensors for three sites within the Caleu pluton. Left: Stereographic projection of ellipsoids axes; large symbols correspond to tensorial mean values determined with the Jelinek's method (1978). Right: Plot of foliation (kint/kmin) versus lineation (kmax/kint); star is the tensorial mean of the site's AMS ellipsoid. Triaxial tensors are observed at site 1. Pencil shapes are observed at site 3 with a large dispersion of minimum susceptibility axes within a plane orthogonal to the lineation direction defined by the maximum susceptibility axes. A well-defined foliation is observed at site 35.

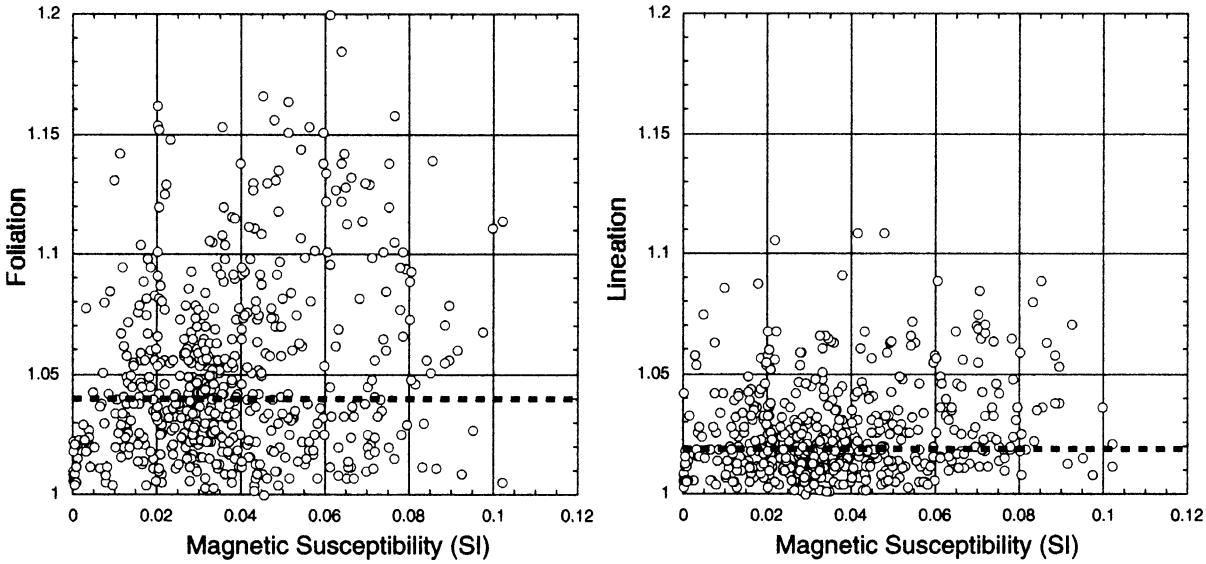

Fig. 8. Plot of the foliation (left) and lineation (right) parameters versus magnetic susceptibility for all the measured samples. The dashed lines correspond to the median foliation and lineation values (4% and 2%, respectively). There is no relation between magnetic susceptibilities and the shape of the AMS ellipsoids.

anisotropies are mostly observed along the eastern side while the largest values are found along the southwestern border and along the contact between GDZ and TZ (Fig. 9). The shapes of AMS ellipsoids are mostly oblate as represented in a Flinn diagram (Fig. 10). Dips of the magnetic foliation planes are steep within the GDZ and TZ while moderate to shallow dips are observed in GZ (Figs. 10 and 11). Magnetic lineations are often in the down direction of the foliation plane and the largest lineation values correspond to steep lineations within subvertical foliation planes.

Magnetic foliations along the southern and eastern border of the pluton are parallel to the corresponding margins. Similar parallelism is observed between the magnetic foliations and the contact between zones, particularly between GDZ and TZ. The magnetic foliations parallel the NW–SE fault contact with the Lo Prado and Veta Negra country rocks. The associated steep magnetic lineations are consistent with the nearly vertical stretching lineations measured in the field.

The distribution of the magnetic foliation within the central part of the TZ and GZ gives rise to lobe-like structures (Fig. 11), associated with the mechanism of emplacement. Unlike the steep fabric observed in the TZ lobe, magnetic foliations of GZ dip gently toward the NE. Note that the curved distribution of the foliation strikes that define the TZ lobe coincides with the shape of the present-day topography (Fig. 11), suggesting that topography mimics the contact between the pluton and its cover.

7. Construction of the Caleu pluton

7.1. Rate of magma ascent

Diapirism and diking (Weinberg and Podladchikov, 1994; Petford, 1996) are the mechanisms that can be invoked for the Caleu magma ascent from the source region to the site of emplacement. The efficiency of each mechanism depends on the deformational behavior of the rocks in the pathways of plutons towards the structurally higher level of emplacement. Because diapiric ascent is more efficient in ductile environment, diking appears to be the mechanism whereby the Caleu magma was transported upward through the brittle upper crust where it was emplaced. Field evidence of diapirism

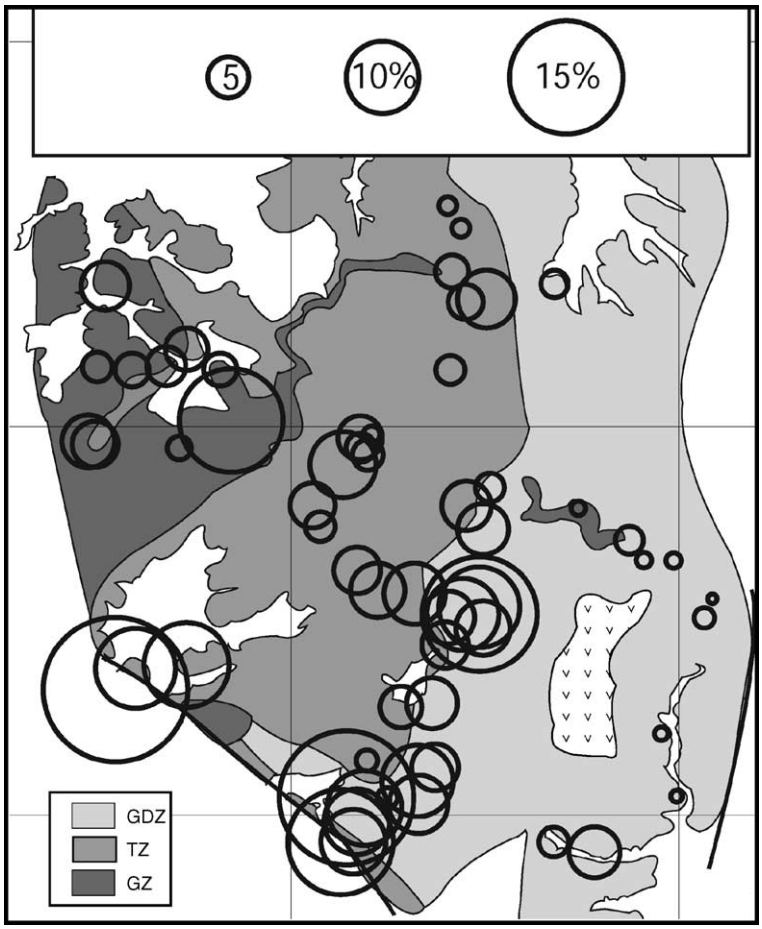

Fig. 9. Map of the AMS intensity. Symbol size is a function of the AMS intensity.

such as deflections of surrounding rocks and large lateral displacement of ductile country rocks by the intrusion are not observed. Moreover, the N–S elongated shapes of the zones observed in the plan view of the pluton (Fig. 1) suggest the presence of feeder dikes parallel to the Andean N–S regional structures. Similarly, the distribution of the steep magnetic foliations following the contact between GDZ and TZ (Fig. 11) suggests a liquid-state feature associated with a N–S feeder.

Magma ascent via dike propagation implies an extremely rapid process. Velocities of granite dike propagation of the order of 10^{-2} m/s have been estimated (Clemens and Mawer, 1992; Petford et al., 1993). Presence of early magmatic epidote in rocks of the GDZ and TZ is an indirect indication of a fast Caleu magma ascent. In fact, based on dissolution kinetics of magmatic epidote, Brandon et al. (1996) showed that to prevent complete epidote resorption, a rapid upward magma transport by dikes is needed. The minimum rate of magma ascent of the Caleu pluton can be estimated from the tonalite samples where early magmatic epidote armored by quartz displays partially resorbed rims. Based on interpolations of the experimental results of Schmidt and Thompson (1996) obtained under oxygen fugacities between NNO and HM and H_2O-saturated conditions, a pressure of about 500–600 MPa is the minimum estimate for the stability of early epidote enclosed in quartz. Thus a decompression of about 300 to 400 MPa, i.e. ~11–15 km of upward magma transport, can be calculated

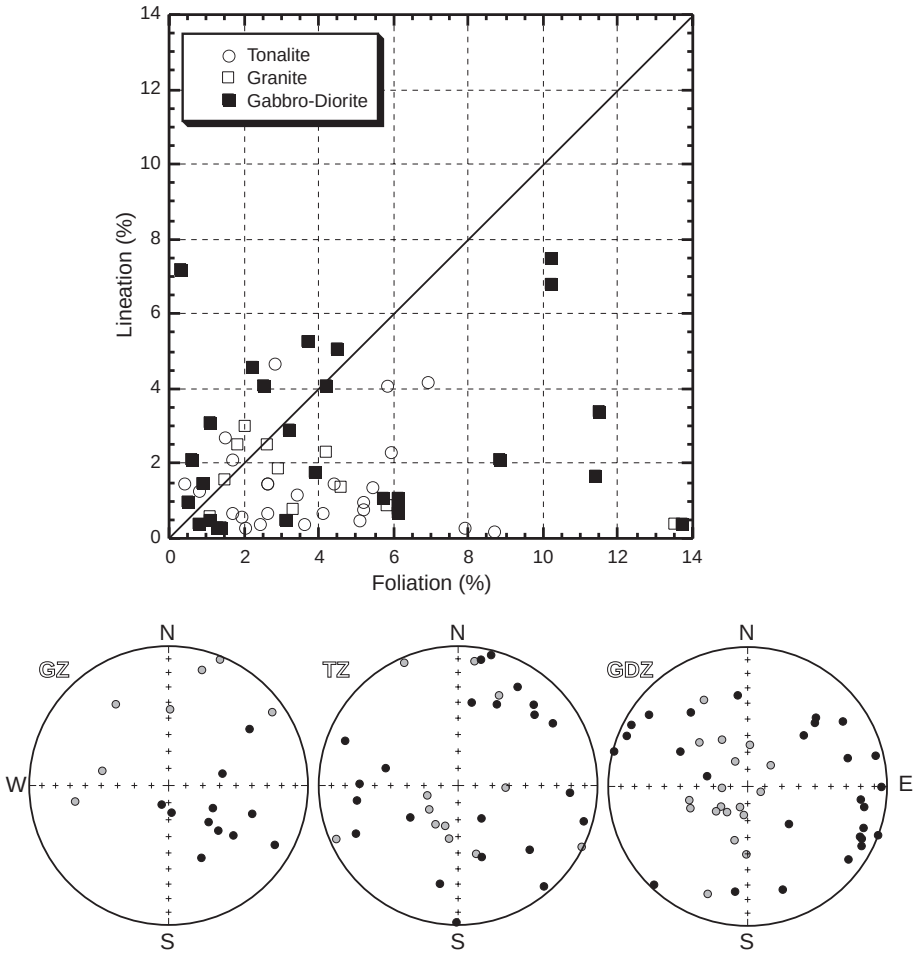

Fig. 10. Top: Flinn type diagrams for the site-mean values. The three units composing the pluton show the same large variation of AMS characteristic. AMS is not controlled by rock composition. Bottom: Equal-area projections of poles of magnetic foliation (black filled circles) and magnetic lineations (grey filled circles) when L>1%. Except in GZ, magnetic lineations are steep.

between crystallization of the epidote+quartz and late magmatic hornblende (~200 MPa; Al-in-hornblende determination). Using the apparent diffusion coefficient of elements between tonalite melt and magmatic epidote (Brandon et al., 1996), a resorption of ~0.2 mm observed in few epidote crystal rims would be completed in 2.5 years. This would imply a rate of ascent of about 1.5×10^{-4} m/s for a decompression equivalent to 11–15 km. Since most of the magmatic epidotes from GDZ and TZ do not show resorption features at their rims, the enclosing magma could have undergone still faster ascent. Note that such high rates of magma ascent typically fall within the values that are envisaged for magma transport by dikes (Clemens and Mawer, 1992; Petford et al., 1993).

7.2. Emplacement by multiple injection and inflation

7.2.1. Mechanisms for the Caleu pluton growth

The space for pluton development is mainly explained by stoping, roof lifting, floor depression or a combination of them (Cruden, 1998; Grocott et al., 1999; McNulty et al., 2000). In the case of the Caleu pluton wall-rock xenoliths were not found, suggesting that stoping would not have played a

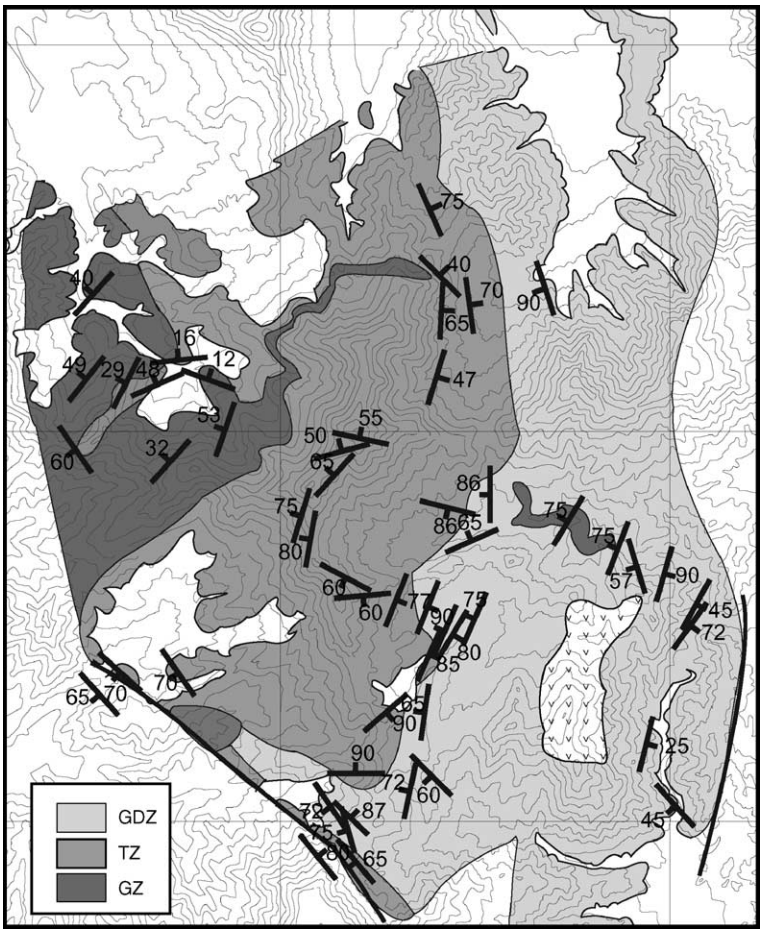

Fig. 11. Map of the AMS foliations. Values correspond to the dip value of the foliation plane. Shallow foliations are observed within the GZ while steep foliations are observed near the southwestern border of the pluton. Foliation planes also tend to parallel the topography.

significant role as a mechanism of space creation. We think that roof lifting and floor depression would have operated. Roof rocks close to the eastern margin of the pluton are found at about 1200 m lower than the highest exposures of the pluton, which are located in its central part (El Roble hill; Fig. 1), suggesting that roof inflation could explain such a difference of this magnitude. Moreover, penetratively deformed host rocks recording vertical displacement attributed to pluton inflation are identified along the southwestern margin (Fig. 1), where nearly vertical magnetic foliations and lineations are also recorded in the marginal rocks of the pluton.

Inflation of the Caleu pluton is also suggested by the lobe-like structure delineated by the circular outward-dipping magnetic foliation measured in TZ at the pluton center (Fig. 11). The inflation of the roof was probably generated by late pulses that pushed up earlier ones. Evidence of this can be obtained from the geochemical stratigraphy of the pluton along a vertical cross section (Fig. 1 and Table 3; see Parada et al., 2002) of about 1400 m elevation in the lobe-like structure of the TZ. A compositional boundary was identified separating two sections with similar vertical compositional gradients (Fig 12). The lower section consists of about 800 m of vertical exposure of mafic enclave-

Table 3
Geochemical compositions

Sample	970121-4	CA-99-2	980124-18	970120-1	970525-1	CA-99-5	CA-99-6	980124-15	980124-12	980124-3	970524-4	970524-3	970120-3	970120-4	970612-2	970118-3	970612-1	970118-6	CA-99-1
Zone	TZ	TZ	TZ	TZ	TZ	TZ	TZ	TZ	TZ	TZ	TZ	TZ	TZ	TZ	GDZ	GDZ	GDZ	GDZ	GDZ
SiO_2	59.80	61.20	65.82	63.30	59.65	58.63	60.45	64.90	54.05	65.30	56.03	60.30	61.59	60.90	62.25	57.20	55.60	53.80	51.63
TiO_2	0.80	0.71	0.51	0.55	0.78	0.77	0.80	0.54	0.75	0.49	0.92	0.78	0.71	0.79	0.79	1.08	1.24	0.56	1.67
Al_2O_3	16.95	17.62	15.92	16.52	16.86	17.03	16.98	15.95	18.68	16.05	17.76	16.95	16.49	17.10	17.17	17.51	18.16	19.50	17.69
Fe_2O_3	1.96	2.26	1.83	2.01	2.19	2.96	2.25	2.04	2.25	1.89	2.69	2.25	2.20	2.46	2.36	2.95	2.20	3.11	3.42
FeO	4.00	3.84	2.80	3.44	4.00	3.36	4.16	3.28	5.32	2.92	5.28	4.12	3.60	4.12	2.28	3.64	4.56	3.20	6.52
MnO	0.11	0.11	0.10	0.09	0.09	0.10	0.09	0.10	0.17	0.07	0.14	0.11	0.12	0.13	0.09	0.12	0.12	0.08	0.17
MgO	2.93	2.17	1.77	2.03	2.93	3.19	2.62	1.90	4.33	1.70	3.64	2.96	2.45	2.59	1.38	2.92	3.40	3.81	4.55
CaO	5.55	4.75	4.18	4.20	5.36	5.31	5.13	4.10	7.65	4.00	6.71	5.63	4.73	4.76	3.24	5.65	6.69	8.70	8.17
Na_2O	4.02	4.21	4.00	4.10	3.73	4.20	3.82	3.96	3.81	3.90	3.77	3.88	3.78	3.51	3.78	4.43	4.43	4.80	3.79
K_2O	2.60	2.33	2.12	2.34	2.63	3.13	2.46	2.26	1.63	2.40	1.59	2.36	2.92	2.46	5.56	3.27	2.42	0.69	1.16
P_2O_5	0.16	0.14	0.13	0.17	0.13	0.13	0.17	0.13	0.09	0.12	0.18	0.16	0.13	0.12	0.19	0.28	0.31	0.32	0.48
LOI	0.78	0.60	0.71	0.88	1.20	0.86	0.94	0.61	1.14	0.92	1.21	0.28	0.92	1.01	0.73	0.67	0.73	1.04	0.63
Total	99.66	99.94	99.89	99.63	99.55	99.67	99.87	99.77	99.87	99.76	99.92	99.78	99.64	99.95	99.82	99.72	99.86	99.61	99.88
Elevation, m	850	1330	1470	1500	1500	1500	1640	1665	1690	1890	1900	1975	2075	2170	1500	1410	1425	1500	1100
Traverse	V	V	HV	HV	H	H	H	V	V	V	V	V	V	V	H	H	H	H	H

Major elements composition for samples of the vertical (V) and horizontal (H) traverses through the Caleu pluton. Most selected samples of the horizontal traverse were collected at elevations between 1400 and 1500 m.

rich tonalites. The upper section is substantially formed by enclave-free diorites and quartz-diorites. Although the upward-increasing silica content and decreasing MgO content observed within each section (Fig 12) are compatible with a convective differentiation process, the stratigraphic sequence of a felsic and lighter section underlying a more mafic and dense section contradicts the gravitational order we expect to find, and is best explained by a tonalitic intrusion nested into a previous more mafic pulse. The mafic enclaves in the tonalites are crude testimonies of mingling between the intrusions,

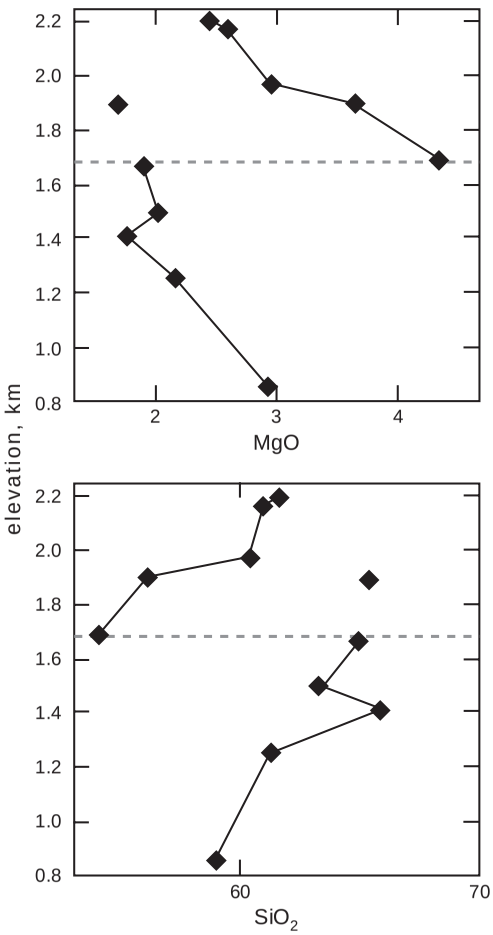

Fig. 12. Compositional variations along a vertical traverse in the TZ (Fig. 1). Samples were taken at elevations between 850 m and 2200 m (Table 3). Geochemical sampling sites do not always correspond to paleomagnetic sampling sites. Dashed line indicates the position of the compositional boundary mentioned in the text.

particularly if one considers that the larger volume of enclave is observed in the proximity of the compositional boundary with the upper section.

Floor depression is assumed considering the presence of a subjacent reservoir from which the Caleu pluton was derived (Parada et al., 2002). We envisage a mechanism of floor depression similar to that proposed for the Mount Givens pluton (Sierra Nevada Batholith; McNulty et al., 2000), whereby melts from the reservoir were induced to ascent by downdrop of the overlying fracture-bounded blocks (Fig. 15c). In this scenario, the magnitude of the downdrop of the overlying block equates the volume of the ascending magma from the subjacent reservoir. The resulting pluton shape would be tabular and its thickness can be estimated at about 6 km by using the empirical power law that relates thickness and horizontal long axis of plutons (McCaffrey and Petford, 1997). This thickness is comparable with those observed in tilted sections of other cordilleran batholiths (Cruden, 1998).

7.2.2. Compositional evidence for pluton growth by episodic injections from a stratified reservoir

According to Parada et al. (2002) the Caleu pluton derived from a common source, each zone having its own geochemical evolution. Fig. 13 shows that rocks from GDZ are more depleted in MgO and Sc, and more enriched in alkalis than rocks from TZ, therefore making unlikely direct derivation of TZ from GDZ. The same conclusion emerges for GZ with respect to TZ by considering their independent plots in Fig. 13. These distinct compositions of GDZ, TZ and GZ have not been acquired in situ but in a deeper (probably at the depth where magmatic epidote crystallized) stratified sill-like reservoir (Parada et al., 2002), which would have been filled once the host volcanic succession at the lower crust was tilted. This assumption is based on the same paleomagnetic directions obtained in the pluton and its adjacent host strata dipping 50–90° (sites 2 and 25; see above). The sill-like shape of the reservoir would have resulted from magma storage at the boundary between two successions with contrasting densities as those represented by the older succession of rhyolite tuffs and limestones (Lo Prado Formation) and the overlying 10-km-thick mafic volcanic succession (Veta Negra Formation). The inclination of floor and roof of the reservoir yields strong compositional

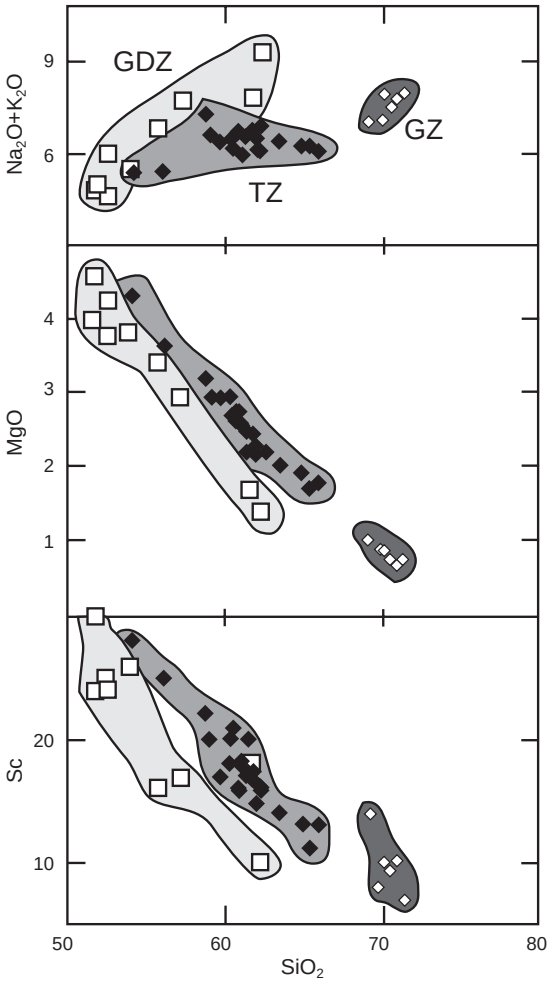

Fig. 13. Selected major and trace elements versus SiO_2 content variation diagrams from the Caleu pluton.

gradients (Huppert et al., 1986). Accordingly, in the assumed eastward-dipping sill-like reservoir of Caleu pluton, the more felsic (lighter) magma occupies the top (western position) and the more mafic (denser) magma ponded at the base (eastern position).

Each zone was likely fed episodically from its respective reservoir (Fig. 15a–c), considering the westward progression of the zone emplacement with time evidenced by the already mentioned intrusive relationships observed in the field. Geochemical compositions (Table 3) obtained from pluton samples collected along a subhorizontal traverse display a compositional break across the contact between the GDZ and TZ (Fig. 14). Similar break can be observed between TZ and GZ.

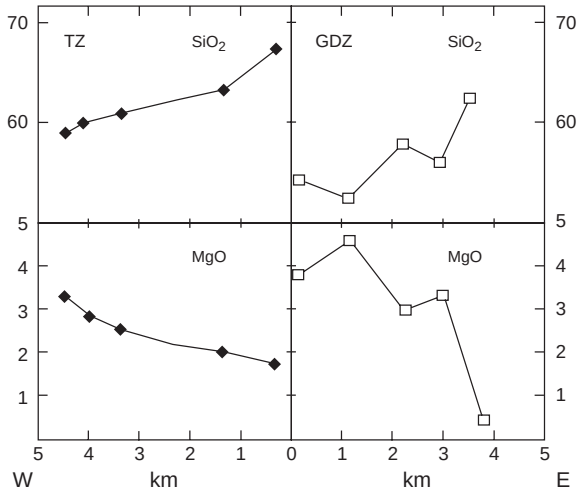

Fig. 14. Compositional variations along a subhorizontal traverse (Fig. 1) across the GDZ (right side)–TZ (left side) boundary. Most selected samples were collected at elevation between ~1400 and 1500 m (Table 3).

These breaks strongly reinforce the hypothesis that both zones were formed by distinct magma batches. The GDZ and TZ feeders would be located roughly beneath the contact area between the two zones (Fig. 15b,c) as suggested by the, already mentioned, steep magnetic foliations subparallel to the contact.

Considering that the compositional variation within a zone reflects the stratification of its reservoir rather than in situ differentiation, the eastward-increase in silica content observed in a horizontal compositional traverse in the GDZ away from the feeder (Fig 14) could result from both magma extraction at progressively deeper levels of the reservoir, and intrusion of later and more mafic magma pulses pushing earlier and more felsic magmas laterally (eastward) away from the feeder system. Similar mechanism may explain the westward decreasing silica in the TZ away from its feeder, but in this case the earlier intrusions representing magmas extracted from deeper levels of the reservoir were pushed westward by late and more felsic injections (Fig. 15b).

8. Conclusions

Paleomagnetic results from the Caleu pluton show no evidence for significant post-emplacement deformation. The difference between the observed and the expected declination, according to the accepted APWP of this area, suggests that the whole area was rotated by about 10 to 20° clockwise since pluton emplacement, without substantial variation in inclina-

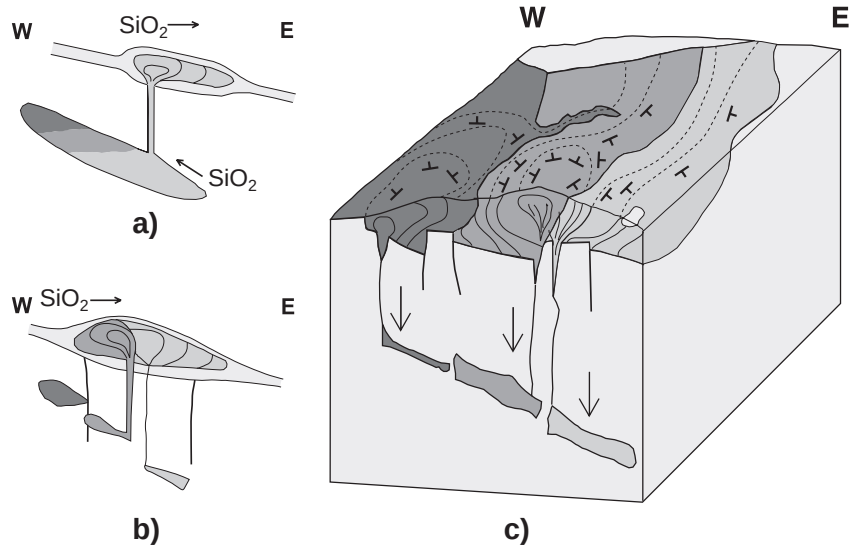

Fig. 15. Conceptual model of evacuation of a zoned reservoir and episodic emplacement by lateral magma spreading and inflation. (a) Initial stage of GDZ emplacement by eastward lateral intrusions. The eastward-increasing SiO_2 content observed within the zone would be a consequence of evacuation of progressively deeper level of its magma reservoir; (b) evacuation and westward lateral emplacement of the TZ; (c) present-day configuration of the pluton. See text.

tion. The pluton intruded the volcanic strata after their tilting to the east.

In contrast with numerous studies showing syntectonic emplacement of plutons (Brown and Solar, 1998, 1999, Wilson and Grocott, 1999; Bouchez, 2000; Archanjo et al., 2002), the magnetic foliations and lineations for the Caleu pluton do not register regional transpressive strain. Rather, they provide insight into the local conditions of emplacement of the Caleu pluton. They also indicate that the NW–SE fault zone that parallels the southwestern edge was associated with the inflation of the pluton during its emplacement. The subvertical N–S contact between TZ and GDZ evidenced by the magnetic foliation indicate that the magma was channelled parallel to N–S regional faults. Lobe-like structures defined by magnetic foliations are indications of magma pulses during the pluton growth.

Finally, taking into account the following facts, among others: (i) the westward progression of the zone emplacement with time, (ii) the compositional variations along a horizontal traverse in the GDZ and TZ, and (iii) the lobe-like structures (pulses) defined by the magnetic foliations, we propose a scenario for the growth of the Caleu pluton consisting in an episodic zone emplacement by combining the effects of magma chamber inflation and laterally spreading magma flow. Correlation between the magnetic foliation pattern and the present-day topography may partially reflect the shape of the pluton roof and its later influence on the geomorphological evolution of this part of the Coastal Range of central Chile.

Acknowledgments

This research was supported by FONDECYT Grant 1990980. We acknowledge the helpful comments and suggestions given by the reviewers J.-L. Bouchez and S. Gilder.

References

Archanjo, C.J., Trindade, R.F., Bouchez, J.-L., Ernesto, M., 2002. Granite fabrics and regional-scale strain partitioning in the Seridó belt (Borborema Province, NE Brazil). Tectonics 21 doi:10.1029/2000TC001269.

Beck, M.E., 1998. On the mechanism of crustal block rotations in the Central Andes. Tectonphysics 299, 75–92.

Benn, K., Odonne, F., de Saint Blanquat, M., 1998. Pluton emplacement during transpression in brittle crust: new views from analogue experiments. Geology 26, 1079–1082.

Besse, J., Courtillot, V., 2002. Apparent and true polar wander and the geometry of the Geomagnetic Field in the last 200 million years. J. Geophys. Res. 107 (B11), 1–31 (EPM 6).

Bouchez, J.-L., 1997. Granite is never isotropic: an introduction to AMS studies of granitic rocks. In: Bouchez, J.-L. (Ed.), Granite: From Segregation of Melt to Emplacement Fabrics. Kluwer Acad. Publ, Dordrecht, pp. 35–38.

Bouchez, J.-L., 2000. Anisotropie de susceptibility magnétique et fabrique des granites. C.R. Acad. Sci. Paris, Sci. Terre Planètes 330, 1–14.

Bouchez, J.-L., Delas, C., Gleizes, G., Nédélec, A., Cuney, M., 1992. Submagmatic microfractures in granites. Geology 20, 35–38.

Brandon, A.D., Creaser, R.A., Chacko, T., 1996. Constraints on rates of granitic magma transport from epidote dissolution kinetics. Science 271, 1845–1848.

Bridgewater, D., Sutton, J., Watterson, J., 1974. Crustal downfolding associated with igneous activity. Tectonophysics 21, 57–77.

Brown, E.H., McClelland, W.C., 2000. Pluton emplacement by sheeting and vertical ballooning in part of the southeast Coast Plutonic Complex, British Columbia. Geol. Soc. Am. Bull. 112, 708–719.

Brown, M., Solar, G.S., 1998. Granite ascent and emplacement during contractional deformation in convergent orogens. J. Struct. Geol. 20, 1365–1393.

Brown, M., Solar, G.S., 1999. The mechanism of ascent and emplacement of granite magma during transpression: a syntectonic granite. Tectonophysics 312, 1–33.

Clemens, J.D., Mawer, C.K., 1992. Granitic magma transport by fracture propagation. Tectonophysics 204, 339–360.

Cruden, A.R., 1998. On the emplacement of tabular granites. J. Geol. Soc. (Lond.) 155, 853–862.

Cruden, A.R., Launeau, P., 1994. Structure, magnetic fabric and emplacement of the Archean Lebel Stock, S.W. Abitibi Greenstone Belt. J. Struct. Geol. 16, 677–691.

Gilder, S., McNulty, B.A., 1999. Tectonic exhumation and tilting of the Mount Givens pluton, central Sierra Nevada, California. Geology 27 (10), 919–922.

Goguitchaichvili, A., Chauvin, A., Roperch, P., Prevot, M., Aguirre, L., Vergara, M., 2000. Paleomagnetic results from the Miocene Farellones formation: a possible highest paleosecular variation during the Miocene. Geophys. J. Int. 140 (2), 357–373.

Grocott, J., Brown, M., Dallmeyer, R.D., Taylor, G.K., Treolar, P.J., 1994. Mechanism of continental growth in extensional arcs: an example from the Andean plate-boundary zone. Geology 22, 391–394.

Grocott, J., Garde, A.A., Chadwick, B., Cruden, A.R., Swager, C., 1999. Emplacement of rapakivi granite and syenite by floor depression and roof uplift in the Paleoproterozoic Ketilidian orogen, south Greenland. J. Geol. Soc. (Lond.) 156, 15–24.

Huppert, H.E., Sparks, R.S., Wilson, J.R., Hallworth, M.A., 1986. Cooling and crystallization at an inclined plane. Earth Planet. Sci. Lett. 79, 319–328.

Hutton, D.H.W., 1988. Granite emplacement mechanism and tectonic controls: inference from deformation studies. Trans. R. Soc. Edinburgh: Earth Sci. 79, 245–255.

Jelinek, V., 1978. Statistical processing of anisotropy of magnetic susceptibility measured on groups of specimens. Stud. Geophys. Geod. 22, 50–62.

Larrondo, P., 2002. El plutón Caleu en la Cordillera de la Costa de Chile central: variaciones mineralógicas y composicionales y condiciones físicas de su formación. MSc. Thesis, University of Chile, Chile.

McNulty, B., Tobisch, O., Cruden, A., Gilder, A., 2000. Multistage emplacement of the Mount Givens pluton, central Sierra Nevada batholith, California. Geol. Soc. Am. Bull. 112, 119–135.

McCaffrey, K.J.W., Petford, N., 1997. Are granitic intrusions scale invariant? J. Geol. Soc. (Lond.) 154, 1–4.

Myers, J.S., 1975. Cauldron subsidence and fluidization: mechanism of intrusion of the coastal batholith of Peru into its own volcanic ejecta. Geol. Soc. Am. Bull. 86, 1209–1220.

Nédelec, A., Paquette, J.-L., Bouchez, J.-L., Olivier, P., Ralison, B., 1994. Stratoid granites of Madagascar: structure and position in the Panafrican orogeny. Geodyn. Acta 7, 56–58.

Olivier, P., Saint-Blanquat, M., de Gleizes, G., Leblanc, D., 1997. Homogeneity of granite fabrics at the meter and decameter scales. In: Bouchez, J.-L. (Ed.), Granite: From Segregation of Melt to Emplacement Fabrics. Kluwer Acad. Publ, Dordrecht, pp. 113–128.

Parada, M.A., Nyström, J.O., Levi, B., 1999. Multiple sources for the Coastal Batholith of central Chile (31–34°S): geochemical and Sr–Nd isotopic evidence and tectonic implications. Lithos 46, 505–521.

Parada, M.A., Féraud, G., Aguirre, L., Fuentes, F., Morata, D., Vergara, M., Larrondo, P., Palacios, C., 2001. U–Pb, ^{40}Ar–^{39}Ar and Fission-Track Geochronology of the Early Cretaceous Caleu Pluton and its Volcanic Envelope, Coastal Range of Central Chile: Tectonic and Metamorphic Implications, Extended Abstracts, vol. 612–616. Pucón, Chile.

Parada, M.A., Larrondo, P., Guiresse, C., Roperch, P., 2002. Magmatic gradients in the Cretaceous Caleu pluton (central Chile): injections of pulses from a stratified reservoir. Gondw. Res. 5, 307–324.

Petford, N., 1996. Dykes or diapirs? Trans. R. Soc. Edinburgh: Earth Sci. 87, 105–114.

Petford, N., Kerr, R.C., Lister, J.R., 1993. Dike transport of granitoid magmas. Geology 21, 845–848.

Petford, N., Cruden, A.R., McCaffrey, K.J.W., Vigneresse, J.-L., 2000. Granite magma formation, transport and emplacement in the Earth's crust. Nature 408, 669–673.

Schmidt, M.W., Thompson, A.B., 1996. Epidote in calc-alkaline magmas: an experimental study of stability, phase relationships, and the role of epidote in magmatic evolution. Am. Mineral. 81, 462–474.

Skarmeta, J.J., Castelli, J.C., 1997. Intrusión sintectónica del granito de las Torres del Paine, Andes patagónicos de Chile. Rev. Geol. Chile 24, 55–74.

Vergara, M., Levi, B., Nyström, J.O., Cancino, A., 1995. Jurassic and early Cretaceous island arc volcanism, extension and subsidence in the coast range of central Chile. Geol. Soc. Am. Bull. 107, 1427–1440.

Weinberg, R.F., Podladchikov, Yu.Yu., 1994. Diapiric ascent of magmas through power-law crust and mantle. J. Geophys. Res. 99, 9543–9559.

Wilson, J., Grocott, J., 1999. The emplacement of the granitic Las Tazas complex, northern Chile: the relationship between local and regional strain. J. Struct. Geol. 21, 1513–1523.